ELSEVIER

Composites: Part A 30 (1999) 123–131

composites
Part A: applied science and manufacturing

A study on failure prediction and design criteria for fiber composites under fire degradation

Ming Dao*, Robert J Asaro

Division of Structural Engineering, Mail Code 0085, University of California, San Diego, La Jolla, CA 92093, USA

Abstract

Polymer matrix composites can be severely degraded/damaged under thermal loading caused by fire. Fire degradation of fiber composites is a serious concern in large load-bearing structural applications such as ship, piers and bridges. This paper describes results from combined experimental and theoretical studies of compressive failures of polymer-matrix glass-reinforced composites which have undergone fire degradation. The focus of the present paper is on single skin composites. Experimental studies have included structural collapse under combined thermal (i.e. fire) and mechanical loading. Detailed analytical and numerical simulations of panel deformation and collapse show good agreement with the experimental observations. A quantitative methodology for developing the design approach is proposed and discussed with respect to the experimental results and thermal boundary conditions.

Keywords: A. Fibers; Fire degradation

1. Introduction

The research reported in this paper is concerned with the effects of fire on the structural integrity of composite materials. The research is part of a program sponsored under the DARPA MARITECH initiative to develop and implement advanced composites for ship design and construction. Specifically, the work discussed here has focused on the development of a quantitative framework for assessing the degradation of composite material properties and the resulting degradation in the structural integrity of composite structures. Our approach has been to characterize the thermal degradation of elastic–plastic properties of advanced composites, to develop models for their temperature- and time-dependent behavior, and conduct combined experimental–theoretical studies of the behavior of thermally degraded composite structures. An important component of our work is the quantitative description of structural collapse, which can serve as the basis of a design methodology. A detailed background introduction and our first report can be found in Asaro and Dao [1].

The specific materials to be described herein are E-glass fabrics embedded in vinyl-ester resins. The composites are fabricated using a vacuum-assisted resin-transfer molding process (viz. SCRIMP, [2]). Fig. 1 illustrates a simple degradation law to describe the reduction in properties with temperature. The discrete data points represent the measured loss in flexural and tensile stiffness of a 24 oz woven roving E-glass/vinyl-ester composite [3]. As the curve indicates, most structural properties are lost as temperatures approach 130°C. The material degradation represented by Fig. 1 is meant to be the instantaneous decrease in stiffness and strength properties at the temperatures in question (i.e. not the *residual properties*).

Previous studies have employed a more semi-empirical approach to describing failure under combined thermal mechanical loads [4–6]. The approach has been based on the notion of *failure surfaces* which are essentially plots of the time-to-failure of simply loaded panels versus the applied uniaxial stress (normalized with respect to an ambient temperature failure stress) and the incident heat flux. Data was obtained on the temperature dependence of basic mechanical properties such as tensile stiffness and strength along with shear strength. This data indicates degradation behavior similar to that shown in Fig. 1. The approach based on empirically determined failure surfaces, as defined above, does not constitute as true material constitutive theory, although the temperature-dependent stiffness data would be useful to calibrate such a constitutive framework. The approach taken in this study involves the development of a quantitative constitutive framework that could be used to analyze full structural response under arbitrary thermomechanical loadings.

* Corresponding author

1359-835X/99/$ - see front matter
PII: S1359-835X(98)00051-7

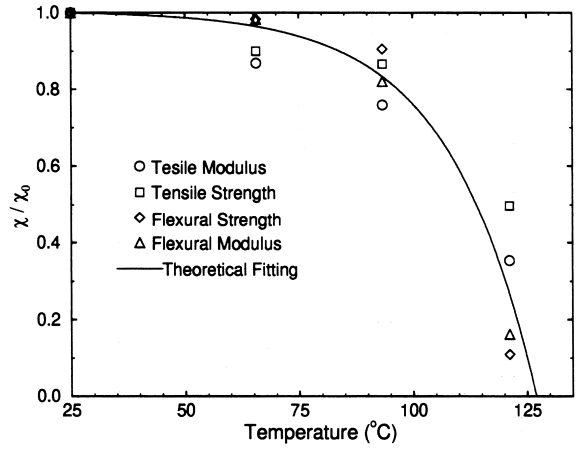

Fig. 1. Property degradation curve; χ and χ_0 represent properties such as stiffness or interlaminar shear strength as they depend on temperature and their initial state respectively.

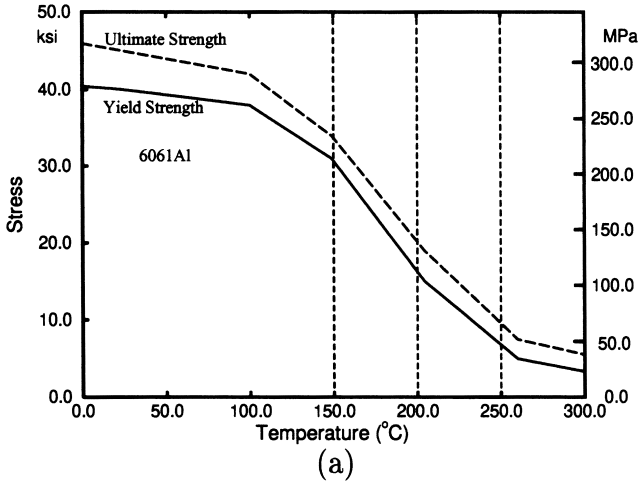

Fig. 2. Elastic–plastic buckling analysis of 6061 aluminum alloy panels: (a) temperature-dependent variation of yield and ultimate tensile strengths, and (b) variations of critical collapse stress, i.e., collapse load averaged over the area of the panel cross-section $P_{coll}/(wh)$.

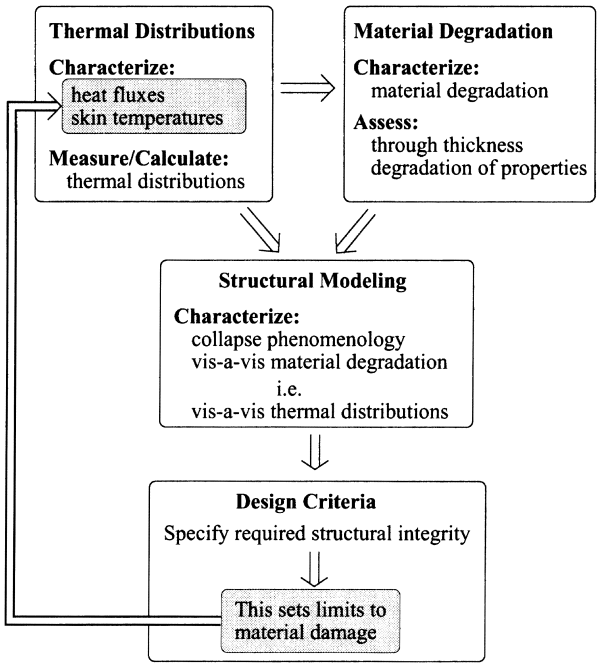

Fig. 3. Modeling approach.

1.1. A discussion on standards for alloy construction

Construction with aluminum alloys generally requires that insulation prevents the 'core' temperatures from exceeding 200°C for the required fire protection time [7]. For perspective, it is useful to attempt to establish a rational basis for such a criterion. To this end, the boundary value problem for an ideal aluminum panel (with rectangular cross-section) subject to uniaxial compressive load is solved. The aluminum alloy panel has the geometry $l \times w \times h$ (length × width × thickness; $w \gg h$), and is pinned at both ends. The tangent modulus method of Shanley [8] is used to calculate the elastic–plastic collapse load. Fig. 2(a) shows the temperature-dependent variation of yield and ultimate tensile strengths of a 6061 aluminum alloy used in the analysis. Fig. 2(b) shows the resulting variations of critical collapse stress, i.e. 'collapse load' averaged over the area of the panel cross-section $P_{coll}/(wh)$. It is obvious that, due to the degradation of strength with temperature, the collapse loads fall rapidly with increasing temperature.

To establish a safety criterion, horizontal lines have been drawn at the levels of 0.5 and 0.67 with the following perspective: original design safety factors of 2 or 1.5 would mean that if the collapse stress would fall below factors of 0.5 or 0.67 of the initial collapse stresses, respectively, all structural safety would be lost as indicated in Fig. 2(b). The temperatures at which this occurs thereby establish threshold temperatures above which (for short times at temperature and neglecting creep deformations) structural integrity is lost. The fact that the temperature range found from Fig. 2(b) is $166°C \leq T \leq 192°C$ helps explain how a

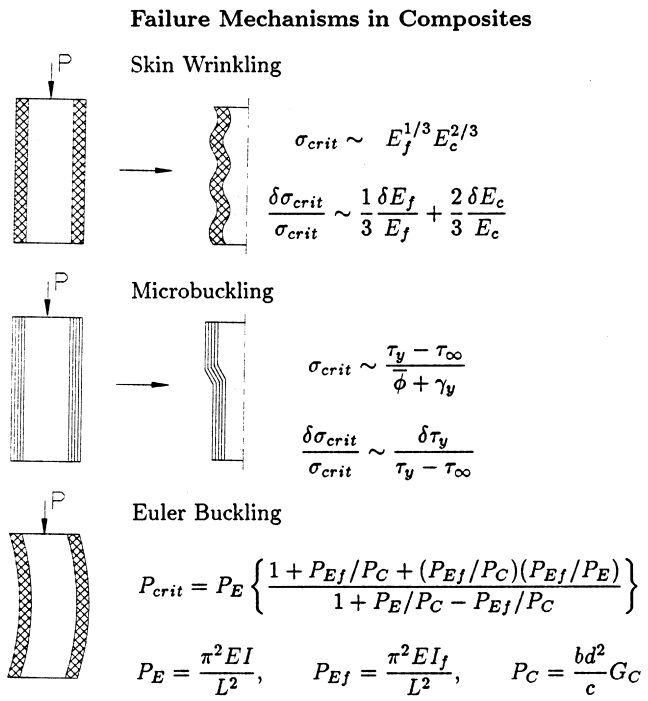

Fig. 4. Failure mechanisms in composites. E_f and E_c are sandwich face and core stiffness respectively. τ_y is the interlaminar shear strength and τ_∞ the remotely applied shear stress. G_c is the in-plane shear stiffness of the core material, and E is again the face stiffness. $\bar{\phi}$ represents an imperfection in the fiber lay-up and is the (assumed small) angle of initial misorientation of axial fiber with the composite axis.

150–200°C temperature limit may be established for aluminum alloy design.

The analysis just described is consistent with the approach outlined in Fig. 3, although the analysis for aluminum alloys would not in itself require such an elaborate description. For composites, however, the process of establishing allowable thermal loads, and thus for establishing required fire protection levels is more complex as discussed next.

1.2. Perspectives on failure in structural composites

Analyses based on aluminum alloys are simpler than those with composites due to (1) reasonably assumed isothermal conditions, and (2) the relative simplicity of the failure mode, viz. uniform thermal degradation of stiffness and strength. There is no assumed, or anticipated, change in failure mode due to elevated temperatures in the case of alloys. Composite materials, on the other hand, possess much lower thermal conductivities (especially in the through-thickness direction) and thus they develop temperature gradients and thereby gradients in stiffness, strength, and physical properties. The analysis of structural failure and the bases for setting allowable limits for thermal loading are accordingly more difficult. Still another reason for the increased difficulty is that the failure modes are more varied and complex as illustrated in Fig. 4. This figure describes three basic material and structural failure processes along with simplified criteria associated with each. Our focus here is on compressive failure processes. The rationale for this is based on the more rapid decrease in resin properties with increasing temperature and the resulting loss in fiber confinement and in interlaminar shear strength. Tension is supported by fibers whose properties are less sensitive to modest temperature elevations.

The strong temperature gradients that develop in either single skin, or cored, composites lead to degradation in the stiffness and strength properties of the composite skins and cores. Examples of thermal gradients in single skin composites are shown later. The extent of these reductions in properties will depend on the detailed manner in which the skin and core material properties change with temperature and the temperature distributions. Which failure mode limits structural integrity will depend on these details, and thus it is possible that a change in failure process could accompany a change in the temperature field. Of course geometry plays, under all conditions, a vital role. For slender panels under compression, structural buckling can easily dominate the failure, which seems to be the case for the panels failure discussed in Section 3.

2. Experimental procedures for panels under compressive loading

The experiments described here were performed under ASTM E119 fire conditions. Panels were thereby subjected to incident time–temperature histories that followed the E119 temperature history. Fig. 5 illustrates the multi-axial loading jig that has been used to apply combinations of in-plane and out-of-plane loads to composite panels.

Two hydraulic rams located on the top edge apply controlled in-plane loads, or displacements, and a single ram located on the unexposed side applies out-of-plane loads or displacements. Out-of-plane loading may be in either direction, i.e. the panels may be deflected into, or away from, the flame. The fixture is bolted onto the rim of a furnace for fire exposure. Displacements are measured on the top edge and along the out-of-plane ram. The panels used in these tests were nominally 0.48 inch (12.2 mm) thick, 36 inch (914.4 mm) long and 28 inch (711.2 mm) wide. They were composed of a 56 oz 5608-08 Quadraxial E-glass fabric, vacuum infused, via SCRIMP, in a vinylester matrix; the fiber volume fraction was 55%. The insulation used was a two-layer 8# mineral wool; this represents two, nominally 25 mm thick, panels of insulation on the fire exposed side. This was used to control heat influx into the panels. Looking ahead to Fig. 7(a) and Fig. 10(a), the thermal loading and insulation produced exposed face temperatures as shown.

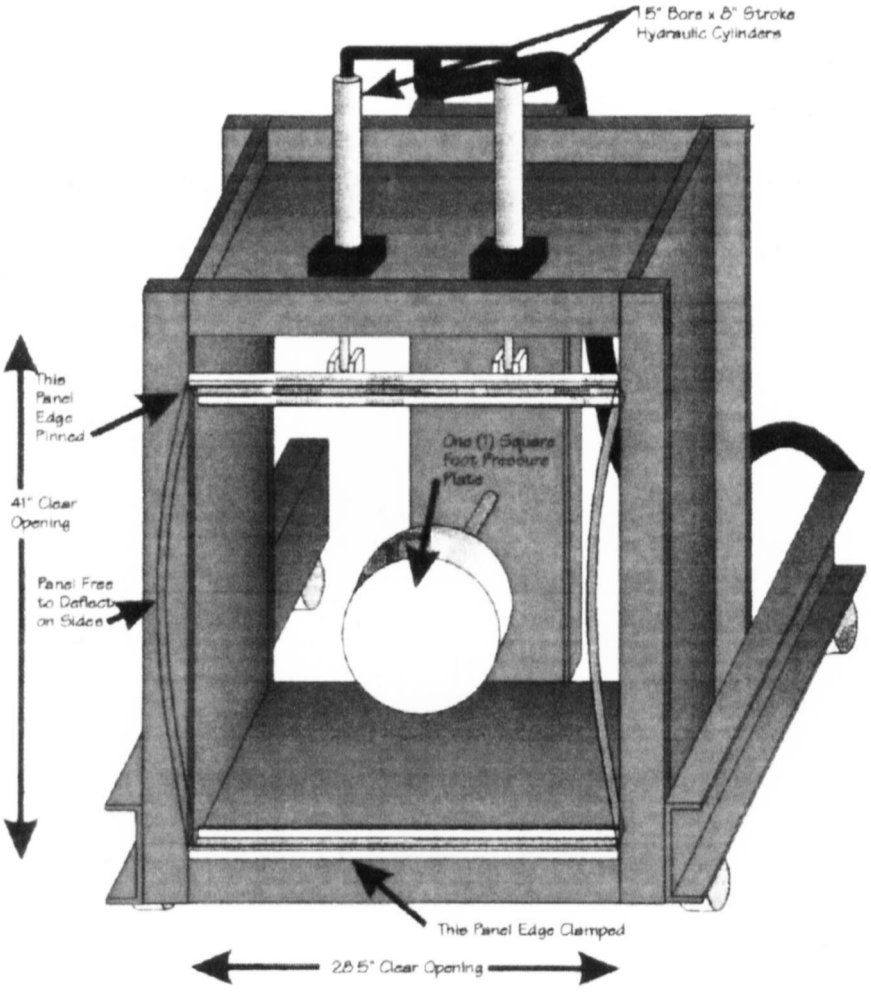

Fig. 5. Multi-axial loading jig.

3. Modeling approach

3.1. A simple collapse model

Here we present a simple model of a single skin composite that has undergone thermal degradation/damage as depicted in Fig. 6. Pin supported end conditions are assumed, and the panel is taken to be subject to symmetrically applied compressive loads. The model does not account for the phenomena of kinking, wrinkling and delamination that may occur and thus attempts only to describe macroscopic collapse via 'buckling like' collapse modes. The model does, however, naturally account for geometrical scaling in terms of panel dimensions.

As a result of an assumed temperature gradient, and the resulting loss in material stiffness, the properties have developed a corresponding gradient as indicated in the figure. Note that the viscoelastic effects at elevated temperatures are not considered here. The material degradation is meant to be the instantaneous decrease in stiffness and strength properties at the temperatures in question. The gradient is assumed to be of the general form

$$\chi = Ax^2 + Bx + C \tag{1}$$

and, with reference to Fig. 6, replacing χ with Young's Modulus E,

$$A = (2\Delta - 4\Delta_1)/h^2,\ B = (4\Delta_1 - \Delta)/h,\ C = E_1$$

$$\Delta_1 = E_c - E_1,\ \Delta = E_2 - E_1 \tag{2}$$

It should be noted, with emphasis, that the collapse loads computed this way depend sensitively on the gradient's form. We also note, in passing, that if $E_c = (E_1 + E_2)/2$ the gradient is linear. In the context of a thermally loaded structure, E_1 would represent the 'exposed face' property (e.g. modulus) and E_2 the 'back face', or 'unexposed face' property. E_c is a property value at the panel's center and whether it is greater or less than $(E_1 + E_2)/2$ determines the shape of the gradient. Before the thermal load begins, $E_1 = E_2 = E_c$; as the exposure time increases, E_1 and then eventually E_c decrease. At longer times the back face temperature elevates and E_2 then also decreases.

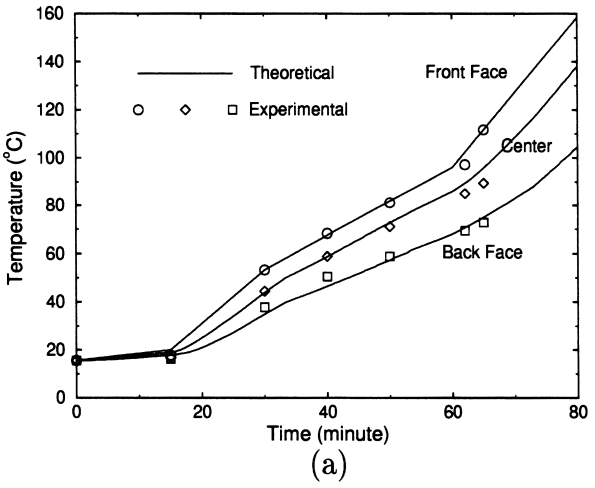

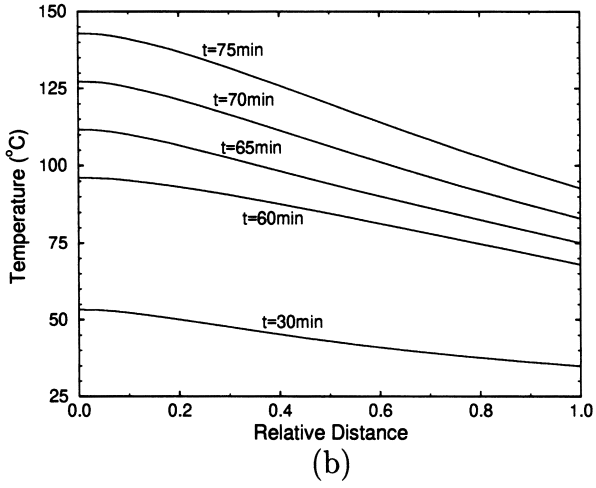

Fig. 7. Thermal analysis results for Case #1: (a) temperature vs. time plots at different panel positions, and (b) temperature distribution profiles at different fire exposure times.

A simple beam theory analysis shows that

$$\frac{P_{\text{coll}}}{P_{\text{E}}} = 1 - \frac{1}{12}\Gamma^2 + \frac{2}{15}\Gamma^- \tag{3a}$$

with

$$\Gamma \equiv \frac{E_2 - E_1}{E_{\text{o}}},\ \Gamma^- \equiv \frac{E_2 - 2E_{\text{c}} + E_1}{E_{\text{o}}}$$

$$E_{\text{o}} = \frac{E_2 + 4E_{\text{c}} + E_1}{6} \tag{3b}$$

P_{E} is an Euler buckling load defined as

$$P_{\text{E}} = \frac{bh^3\pi^2}{12L^2}E_{\text{o}} \tag{4}$$

When $E_{\text{c}} = (E_1 + E_2)/2$ the gradient is linear, $\Gamma^- = 0$, and Eq. (3) becomes

$$\frac{P_{\text{coll}}}{P_{\text{E}}} = 1 - \frac{1}{12}\Gamma^2 \tag{5a}$$

$$P_{\text{E}} = \frac{bh^3\pi^2}{12L^2}E_{\text{o}},\ \Gamma = \frac{E_2 - E_1}{E_{\text{o}}},\ E_{\text{o}} = \frac{E_2 + E_1}{2} \tag{5b}$$

In this linear case, P_{E} is the Euler buckling load for a 'uniform companion panel' with an average of the exposed and back face moduli.

3.2. Micromechanical considerations

The integrated experimental/theoretical approach outlined in Fig. 3 is aimed at developing a quantitative methodology for assessing the structural integrity of composite materials subject to severe thermal loads caused by fire. The approach involves modeling composite material degradation due to fire loads and developing an analytical and computational methodology to describe the loss in load-bearing capacity (i.e. structural integrity) of composite structures. Direct outputs of this specification would be the maximum thermal loads that typical structural members could tolerate for required fire protection times, along with a quantitative framework for assessing structural response during and after a fire (Fig. 3). An end prescription might be a set of relatively simple design models of the type described in Eqs. (3a)–(5b). These models would allow a quantitative assessment of the loss in load-bearing capacity accompanying material damage, which itself is quantitatively linked to thermal profile. It is vital, however, to ensure that these models do not omit critical phenomena or processes, including micromechanical ones, that may control the failures. For this reason we have performed detailed computational studies of compressive failures to compare with experimentally observed failures in our earlier study [1].

The detailed layered structure and the three-dimensional geometry were modeled using three-dimensional layered shell elements, and the three-dimensional finite element analysis with biaxial loading conditions gave practically the same results as our simple two-dimensional model given by Eqs. (3a), (3b) and (4).

Also, detailed kink band analyses were performed to check the possibilities of kinking-type micromechanical failure modes. It was concluded that, unless we took unusually extreme material properties or very large initial imperfections, the single skin panel under fire degradation would fail under the structural buckling mode.

With the above information in mind, we can now apply the model presented in Eqs. (3a), (3b) and (4) for the structural analyses in later sections.

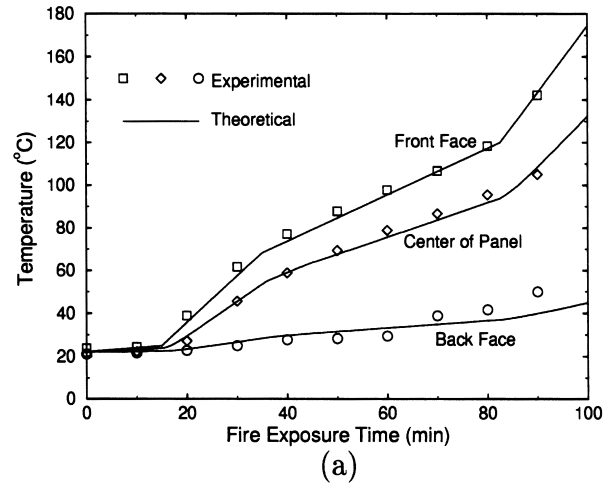

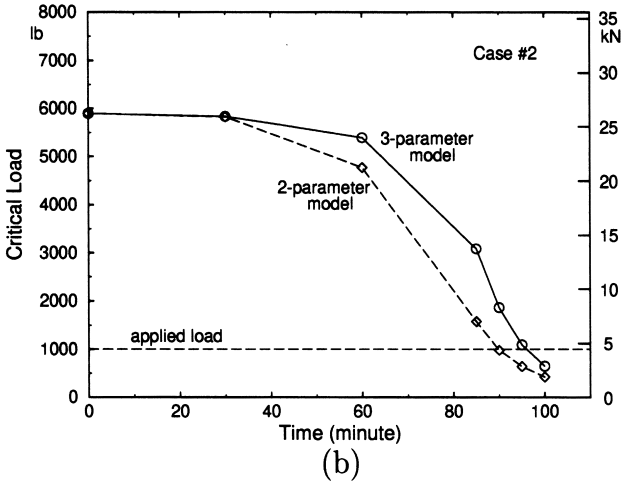

Fig. 10. Analysis results for Case #2: (a) temperature vs. time plots at different panel positions, and (b) critical collapse load vs. fire exposure time.

4. Model analyses results

4.1. Thermal analysis

A finite difference thermal analysis code was used to simulate the temperature distributions. The code is three-dimensional and assumes the thermal conductivities to have orthotropic symmetry. Assuming uniform in-plane temperature distribution, the problem reduces to a one-dimensional simple case. The heat conduction equation is thus

$$\frac{\partial}{\partial x}\left[k(T)\frac{\partial T}{\partial x}\right] = \rho C_\rho \frac{\partial T}{\partial t} \tag{6}$$

where $k(T)$ is the out-of-plane heat conductivity, ρ is the density of the material, C_ρ is the specific heat, T is the temperature, and t is the fire exposure time. The initial condition is given as

$$T(x,0) = T_{\mathrm{RT}} \tag{7}$$

where T_{RT} stands for room temperature. The boundary condition at the fire side is simply given as the measured front face temperature $T_{\mathrm{f}}^{\mathrm{exp}}(t)$

$$T(0,t) = T_{\mathrm{f}}^{\mathrm{exp}}(t) \tag{8}$$

There are two possible boundary conditions at the back side of the panel, i.e. insulated back face

$$\frac{\partial T(x=h,t)}{\partial x} = 0 \tag{9}$$

or constant room temperature at the back face

$$T(x=h,t) = T_{\mathrm{RT}} \tag{10}$$

In reality, neither of the ideal boundary conditions shown in Eqs. (9) and (10) would work well. A simple 'mixture boundary condition' is thus proposed as

$$T(h,t) = \alpha T^{\mathrm{Eq.\ (9)}}(t) + (1-\alpha)T^{\mathrm{Eq.\ (10)}}(t) \tag{11}$$

where $0 \le \alpha \le 1$ is a mixture constant, and $T^{\mathrm{Eq.\ (9)}}(t)$ and $T^{\mathrm{Eq.\ (10)}}(t)$ are the solutions obtained using the boundary conditions of Eqs. (9) and (10) at each current finite difference step respectively.

Fig. 7(a) shows the temperature profiles at various positions on one of the composite test panels. This panel test will

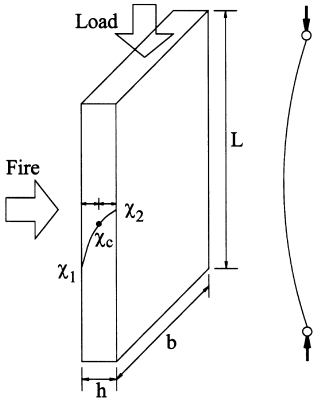

Fig. 6. A simple collapse model with material property variation.

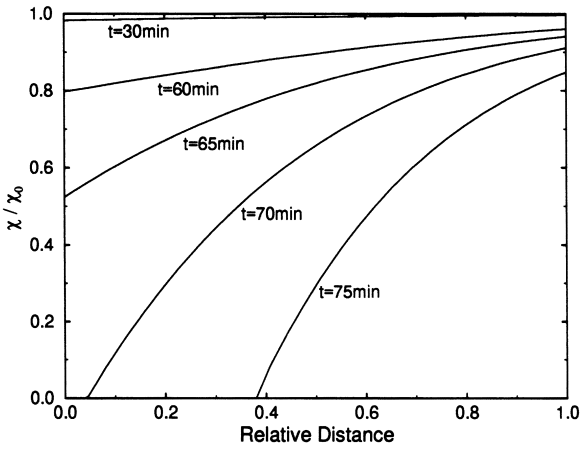

Fig. 8. Through-thickness degradation profiles at different times for Case #1.

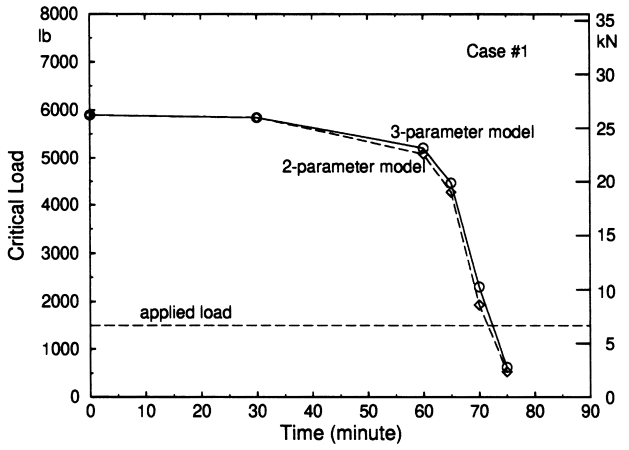

Fig. 9. Critical collapse load vs. fire exposure time plot for Case #1.

hereafter be referred to as Case #1. The theoretical results are in good agreements with the experimental curves. The out-of-plane thermal conductivity k was taken as 0.25 W m^{-1} °C^{-1}, ρ as 1.6 × 10^3 kg m^{-3}, C_ρ as 1.5 × 10^3 J kg^{-1} °C^{-1} and α as 0.5. Fig. 7(b) shows the through-thickness temperature distribution profiles at five different fire exposure times. These more detailed thermal distributions were obtained by interpolating using the theoretically computed temperature profiles.

4.2. Material degradation profile

The next step after the thermal analysis is to determine the property degradation profile vs. temperature. As noted earlier, an ideal property degradation curve obtained by fitting to a measured reduction in flexural and in-plane stiffness was used (see Fig. 1). It is assumed that all components of the elasticity tensor, in addition to the interlaminar shear strength, follow this master degradation curve. It is very clear that before 100°C, the degradation is not significant; after 100°C, the modulus drops rapidly and quickly approaches zero at about 130°C.

With the information available in Figs. 1 and 7(b), through-thickness degradation profiles can be obtained. Fig. 8 shows such a plot of through-thickness degradation profiles at several fire exposure times. It is interesting to note that, at $t = 75$ min, 39% of the material is completely damaged, with zero load-bearing capacity. The progression of damage vs. time is also evident.

4.3. Structural analyses

With all the degraded property profiles in hand, a structural analysis can be performed. Using the model presented in Section 3 (cf. Eqs. (3a), (3b) and (4)), and taking the values E_1, E_2 and E_c as shown in Fig. 8, a critical load vs. time profile can be calculated (see the solid line labeled as 'three-parameter model' in Fig. 9).

With the applied in-plane load at 6.67 kN (1500 lb), the predicted failure time was found at about 72 min. The actual measured failure time was 65 min. Considering the 1.33 kN (300 lb) out-of-plane load applied in the experiment, the match is fairly good. In this approach, we took three engineering parameters (E_1, E_2 and E_c) as input in the model.

4.4. A two-parameter model

After carefully examining the degradation profile shown in Fig. 8, it is clear that the major load-bearing capacity is carried mostly by the unexposed half side of the panel, especially when approaching failure time. Another observation is that, along the unexposed half side, the temperature distribution is quite close to linear during the whole degradation process (see Fig. 7(b)). This means that linear interpolation between T_c and T_b can quite accurately describe the temperature distribution profile of the unexposed half side and therefore fairly accurately describe the load-bearing capacity of the unexposed half side with the help of the master degradation profile (Fig. 1). Here, we define T_f, T_c and T_b as the fire side, center, and back side temperature, respectively. Next, assuming a linear temperature distribution across the whole panel, we estimate T_f by extrapolating from T_b and T_c, e.g.

$$T_f = T_c + (T_c - T_b) = 2T_c - T_b \tag{12}$$

Using the newly computed T_f, together with T_c and T_b, the degradation profile in Fig. 1 can be used to compute E_1, E_c and E_2. Thus, from Eqs. (3a), (3b) and (4), the critical collapse load for the entire panel can be estimated. This model takes two parameters, T_c and T_b, as the input. The result of the two-parameter model is plotted against that of the three-parameter model as shown in Fig. 9. Both models give practically the same failure time prediction for this case, which is about 72 min (close to the measured time 65 min).

This exercise suggests that the center temperature T_c and the back side temperature T_b (strongly influenced by the thermal boundary conditions at the back side) are two of the most influential parameters in structural failure analysis.

4.5. Case #2

This case describes the results of another panel, for which both the thermal and mechanical loadings were less severe than for the panel just reviewed. For this panel the in-plane load was 4.45 kN (1000 lb) and the out-of-plane load was 2.22 kN (500 lb). Thermal insulation was used as described earlier, but the same E119 thermal load resulted in a less severe temperature rise as shown in Fig. 10(a), where the theoretical curve was obtained with $\alpha = 0.1$ in Eq. (11). The procedure described in Sections 4.1, 4.2, 4.3 and 4.4 is then applied. The computed results of critical collapse load vs. fire exposure time for both the three-parameter and two-parameter models are shown in Fig. 10(b), where the estimated failure times are approximately 95 and 90 min, respectively. The experimentally observed time to failure

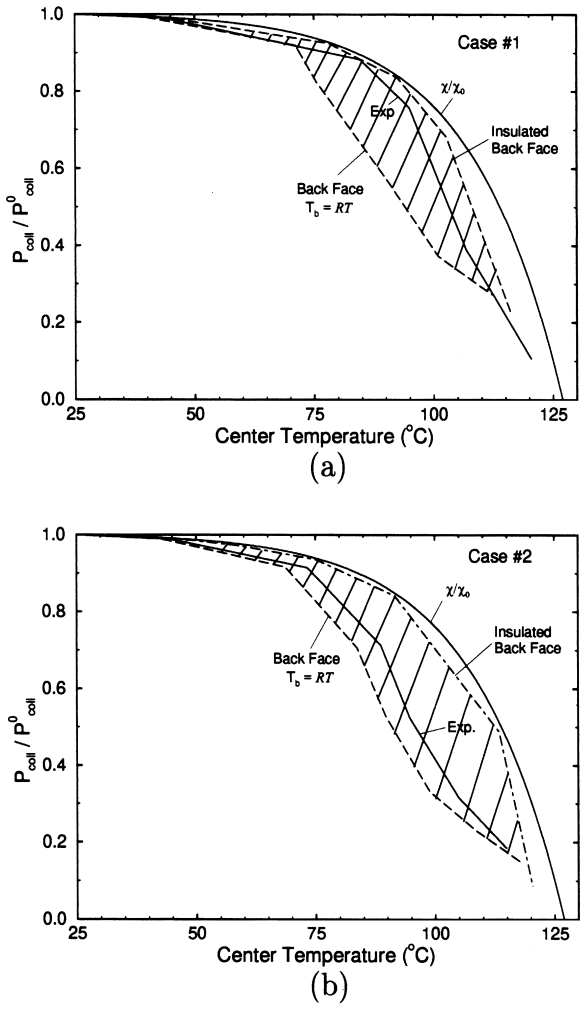

Fig. 11. Critical collapse load vs. center temperature T_c for (a) Case #1, and (b) Case #2.

was approximately 92 min. Again, very good agreement between theory and experiment is found in Case #2 here.

5. A discussion on design criteria

With the two case studies presented in Section 4, we now seek some possible design criteria. Similar to the case for simple metal aluminum, a collapse load vs. center temperature criterion is evaluated.

As discussed earlier in Section 4.4, the center temperature T_c and the back side thermal boundary condition T_b are two of the most influential factors in structural failure analysis. Now we are seeking to understand the relationship of the critical collapse load P_{coll} vs. these two factors.

For Case #1 studied in Figs. 7–9, we first fix the temperature–time history at the front face of the panel, and choose two extreme back face thermal boundary conditions: (1) insulated back face, and (2) the back face temperature $T_b \equiv$ RT (RT is room temperature). The standard procedure described in Sections 4.1, 4.2 and 4.3 is then applied to compute the critical collapse load P_{coll}, and the results are plotted against the center temperature T_c as shown in Fig. 11(a). The master degradation curve is also shown in the figure. The insulated back face curve is seen quite close to the master degradation curve, and the experimental curve is between the two extreme cases but closer to the insulated back face curve.

A similar analysis can be applied to the second panel (Case #2) described in Fig. 10. In Fig. 11(b), the experimental curve is plotted against the results using two extreme back face thermal boundary conditions; the master degradation curve is also shown in the figure. Again, we observe that the insulated back face curve is rather close to the master degradation curve, while the experimental curve is between the two extreme cases but closer to the $T_b \equiv$ RT curve.

From Fig. 11(a) and 11(b), if we shade the areas between the two extreme back face thermal conditions, a ‘danger zone’ can be readily identified for both Case #1 and Case #2. Any load higher than the ‘danger zone’ will not survive the fire damage; any load below the danger zone will be safe; and any load in between will depend on the actual thermal boundary conditions. Another interesting observation is that, although the two cases have quite different thermal/mechanical history vs. time, they have similar ‘danger zones’.

The danger zone approach is conceptually similar to the design criterion used with aluminum alloys as described and discussed in Section 1. The difference is that, for aluminum alloys (simple metals), the danger zone collapses to a single line—the master degradation curve—and a uniform temperature across the panel thickness can be assumed.

Descriptions of failure in cored panels will, for reasons discussed earlier in Section 1, be more complex. For example, skin wrinkling is one such important failure mode to be carefully studied. Experimental studies of structural collapse in cored, i.e. sandwich, panels subject to combined thermal and mechanical loads are currently underway. These are being complemented by detailed computational simulations; the failure mechanisms and criteria listed in Fig. 4 serve as guides. Future work will focus on cored sandwich panels.

Acknowledgements

The authors gratefully acknowledge helpful discussions with Prof. Tian-Hu Hao and Dr. Pei Gu during the course of this study.

References

[1] Asaro RJ, Dao M. Marine Technology 1997;34(3):197–210 Society of Naval Architects and Marine Engineers (SNAME).
[2] Loud S. Composites Technology 1995;1(3):36–41.
[3] McCabe T. Private communication, 1996.

[4] Milke JA, Vizzini AJ. J Comp Tech Res 1991;13:145.
[5] Chang CI. Theoret Appl Fracture Mech 1986;6:113.
[6] Griffis CA, Nemes JA, Stonesifer FR, Chang CI. J Comp Mater 1986;20:216.
[7] International Code of Safety for High-Speed Craft, Chapter 7, International Maritime Organization (IMO), London, 1995.
[8] Shanley FR. J Aero Sci 1947;14:251.